Mutation Induced Modulation of Hydrogen Bonding to P700 Studied Using FTIR Difference Spectroscopy†

Ruili Wang,‡ Velautham Sivakumar,‡ Yajing Li,§ Kevin Redding,§ and Gary Hastings*,‡

Department of Physics and Astronomy, Georgia State University, Atlanta, Georgia 30303, and Departments of Chemistry and Biological Sciences, The University of Alabama, Tuscaloosa, Alabama 35487-0336

Received February 10, 2003; Revised Manuscript Received April 15, 2003

ABSTRACT: Site-directed mutagenesis in combination with Fourier transform infrared difference spectroscopy has been used to study how hydrogen bonding modulates the electronic and physical organization of P700, the primary electron donor in photosystem I. Wild-type PS I particles from *Chlamydomonas reinhardtii* and a mutant in which ThrA739 is changed to alanine [TA(A739) mutant] were studied. ThrA739 is thought to provide a hydrogen bond to the chlorophyll-*a*′ molecule of P700 (the two chlorophylls of P700 ($P700^+$) will be called P_A and P_B (P_A^+ and P_B^+)). The mutation considerably alters the ($P700^+$−P700) FTIR difference spectra. However, we were able to describe all of the mutation induced changes in the difference spectra in terms of difference band assignments that were proposed recently (Hastings, G., Ramesh, V. M., Wang, R., Sivakumar, V. and Webber, A. (2001) *Biochemistry 40*, 12943−12949). Upon comparison of mutant and wild type ($P700^+$−P700) FTIR difference spectra, it is shown that (1) the 13^3 ester carbonyl modes of P_A and P_B are unaltered upon mutation of ThrA739 to alanine. (2) The 13^3 ester carbonyl modes of P_A^+/P_B^+ upshift/downshift upon mutation. These oppositely directed shifts indicate that the mutation modifies the charge distribution over the pigments in the $P700^+$ state, with charge on P_B being relocated onto P_A. We also show that the 13^1 keto carbonyl mode of P_B/P_B^+ is unaltered/downshifted upon mutation, as is expected for the above-described mutation induced charge redistribution in $P700^+$. Although the 13^3 ester carbonyl modes of the chlorophylls of P700 in the ground state are unaltered upon mutation, the 13^1 keto carbonyl mode of P_A upshifts upon mutation, as does the 13^1 keto carbonyl mode of P_A^+. For P700 in the ground state, bands that we associate with HisA676/HisB656 upshift/downshift upon mutation. For the $P700^+$ state, bands that we associate with HisA676/HisB656 also upshift/downshift upon mutation. These observations are also consistent with the notion that the mutation leads to the charge on P_B^+ being relocated onto P_A^+. In addition, we suggest that a hydrogen bond to the 13^1 keto carbonyl of P_A is still present in the TA(A739) mutant, probably mediated through an introduced water molecule.

Photosystem I (PS I)[1] is one of the two light activated enzymes present in the thylakoid membrane of plants algae and cyanobacteria. Light activation of PS I results in the generation of an electrical potential gradient across the membrane. The energy in the electrical potential gradient is harnessed via a series of biochemical processes that ultimately result in the generation of ATP and/or reducing products, which are necessary precursors in a series of dark reactions that lead to carbon assimilation (*1*−*3*). In PS I, the generation of an electrical potential gradient is achieved by the light induced oxidation of a dimeric chlorophyll-*a* species called P700. The electron from the oxidation process is transferred across the membrane via a sequential series of electron acceptors called A_0 (a chlorophyll species), A_1 (a phylloquinone), and F_X (an iron sulfur complex) (*4*). The electron-transfer cofactors in PS I are bound to two membrane spanning proteins called *Psa*A and *Psa*B. In PS I, there are two symmetrical sets of electron carriers bound to *Psa*A and B, and it is unclear if ET occurs down one or both of these symmetrical branches (*5*−*8*). The two chlorophylls that constitute P700 sit at the juncture of the two branches, with a Chl-*a* molecule bound to *Psa*B and a Chl-*a*′ molecule bound to *Psa*A (*9*, *10*). The structure and numbering scheme for Chl-*a* is outlined in Figure 1. Chl-*a*′ is a 13^2 isomer of Chl-*a*. Throughout this paper, the two Chls of P700 are termed P_B and P_A. In the oxidized state ($P700^+$), these Chls are termed P_A^+ and P_B^+.

Although there appears to be a high degree of symmetry in the ET chain in PS I (*9*, *10*), this symmetry does not extend to P700, the primary electron donor. It is therefore likely

† This work was supported by start-up funds, a quality improvement grant, and a research initiation grant to G.H. from Georgia State University. G.H. also acknowledges support from the USDA (Grant 35318-10894). K.R. acknowledges support from the DOE (Energy Biosciences Grant DE-FG02-00ER15097).

* To whom correspondence should be addressed. Phone: (404) 651-0748. Fax: (404) 651-1427. E-mail: ghastings@gsu.edu.

‡ Georgia State University.

§ University of Alabama.

[1] Abbreviations: Chl-*a*, chlorophyll-*a*; *C.*, *Chlamydomonas*; C═O, carbonyl; (D)DS, (double) difference spectra/spectrum or spectroscopy; FTIR, Fourier transform infrared; H-bond, hydrogen bond; PS I, photosystem one; P700, primary donor in PS I; $P_{A/B}$, Chl-*a*′/Chl-*a* of P700 bound to *Psa*A/B; RT, room temperature; SDM, site-directed mutagenesis or mutants; *S.*, *Synechocystis* or *Synechococcus*; His or H, histidine; Thr or T, threonine; Ala or A, alanine.

10.1021/bi034230c CCC: $25.00
Published on Web 07/29/2003

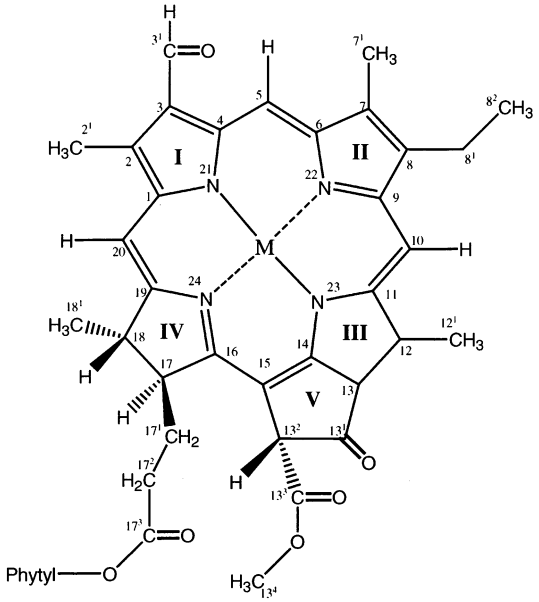

FIGURE 1: Molecular structure and IUPAC numbering scheme for chlorophyll-*a* (Chl-*a*). Chl-*a*′ is a 13^2 isomer of Chl-*a*.

that the electronic and structural organization of P700 is tied to the degree of ET directionality in PS I. The possibility that P700 could modulate ET directionality, and the highly resolved PS I crystal structure (*9*, *10*), has renewed interest in research aimed at investigating the electronic and physical organization of P700.

From the 2.5 Å PS I crystal structure, P_A and P_B are well-resolved (Figure 2, (*9*, *10*)). The two pigments are asymmetrically bound, with P_A being involved in a hydrogen (H) bond network with several surrounding amino acid residues and a water molecule (Figure 2 (*9*, *10*)). P_B is not involved in H-bonding. Figure 2A shows that the hydroxyl oxygen of ThrA743 is 2.98 Å from the 13^1 keto carbonyl (C═O) oxygen of P_A. In addition, the ThrA743 hydroxyl oxygen is 2.7 Å from the oxygen atom of a water molecule (H_2O-19). If ThrA743 is oriented such that its hydroxyl group provides an H-bond to the 13^1 keto C═O of P_A, then the lone pair of electrons on the hydroxyl oxygen of ThrA743 are well-positioned for H-bonding with H_2O-19. Importantly, the strength of the H-bond provided by ThrA739 to the 13^1 keto C═O of P_A is dependent on the proton from H_2O-19 pointing toward ThrA739. H_2O-19 could also be involved in H-bonding to the backbone oxygen of GlyA739 (Figure 2C,D), the side chain O−H of TyrA603 (Figure 2E), or the backbone oxygen of SerA607 (Figure 2F). H_2O-19 and TyrA603 could also be H-bonded to the bridging ester oxygen of P_A. We also note that ThrA743 could be H-bonded to the bridging ester oxygen of P_A (Figure 2A,C). The 13^3 ester C═O of P_A appears to be free from H-bonding. Finally, TyrA735 could be H-bonded to the 17^3 ester C═O of P_A or to the backbone of SerA607. In Figure 2, the *S. elongatus* amino acid numbering scheme was used. All of the amino acids in Figure 2 are conserved in *Chlamydomonas reinhardtii* and are numbered; TyrA600, SerA604, TyrA731, GlyA735, and ThrA739. In addition, in *C. reinhardtii*, the axial histidines to P_A and P_B are HisA676 and HisB656, respectively. We will use *C. reinhardtii* numbering throughout this paper.

Removal of ThrA739, and the possible H-bond to the 13^1 keto C═O of P_A, could disrupt the H-bond network, which could alter the properties of P700. To investigate these altered properties, we have constructed a site-directed mutant from *C. reinhardtii* (strain P71, see Materials and Methods) in which ThrA739 has been changed to alanine. This mutant is termed the TA(A739) mutant. The preferred orientation of substituted Ala(A739) is shown in Figure 2B. At present, it is unclear if P_A in *C. reinhardtii* PS I is a Chl-*a*′. It is also unclear if P_A is a Chl-*a*′ in the mutants in which ThrA739 has been substituted, although Witt et al. (*11*) claim to have determined (unpublished) that one Chl-*a*′ molecule is present in their WT PS I particles from *C. reinhardtii* and in all mutant PS I particles in which ThrA739 has been substituted. This suggests that P_A is a Chl-*a*′ in both WT and TA(A739) mutant PS I particles.

Here, we have used ($P700^+$−P700) FTIR difference and double difference spectroscopy (DDS) to analyze mutation induced alterations in the molecular and electronic structure of P700 and $P700^+$. Witt et al. also produced ($P700^+$−P700) FTIR DS for their ThrA739 site-directed mutants. However, these authors did not produce FTIR DDS and provided only a partial and incomplete interpretation of their spectra.

MATERIALS AND METHODS

Site-Directed Mutagenesis. The point mutations were created as described (*12*). After sequencing to confirm the point mutations, the plasmid DNA was coated onto 1-μm diameter gold particles and introduced into algae chloroplast ballistically. The recipient strains of *C. reinhardtii* were KRC91 (*P71 FUD7 psaA*Δ) or KRC94 (*P71 FUD7 psaB*Δ), which had no PS II and lowered antenna content to simplify PS I purification for biophysical analyses. Transformants were selected by resistance to the antibiotics spectinomycin and streptinomycin. The mutations within the transformants were confirmed by PCR using purified genomic DNA as the template. The control strain (wild type) KRC1003 was made by crossing a *nac2* strain with a *P71* strain to create a *nac2 P71* double mutant, containing no PS2 and lowered amounts of light harvesting complexes. Cells were grown in Tris-acetate-phosphate medium (*13*) at 25 °C in low light. Thylakoid membranes and PS I particles were prepared as described (*7*).

For all FTIR experiments, PS I particles were pelleted and placed between a pair of CaF_2 windows. No mediators were added, although identical spectra were obtained in the presence of a mixture of ferri/ferrocyanide (data not shown). All experiments were performed at room temperature. FTIR spectra were recorded using a Bruker IFS/66 FTIR spectrometer. Spectra were collected before, during, and after light excitation from a helium−neon laser, as described (*14*). All spectral analyses (subtractions, second derivative calculations, Fourier deconvolution, and curve fitting) were performed using the software package OPUS, supplied by Bruker Instruments. No smoothing procedures were applied to any of the data presented here. Data were collected using 4 or 2 cm^{-1} resolution. In spectra collected at 2 cm^{-1} resolution, a data point is collected every 0.62 cm^{-1}. For Fourier deconvolution of the spectra, the following variables were used: bandwidth, 1.0 and resolution enhancement, 8 (deconvolution factor, 535; noise reduction factor, 4.5). In all deconvolved spectra, no sign of spurious bands, or bands due to water vapor, were observed in any spectral region,

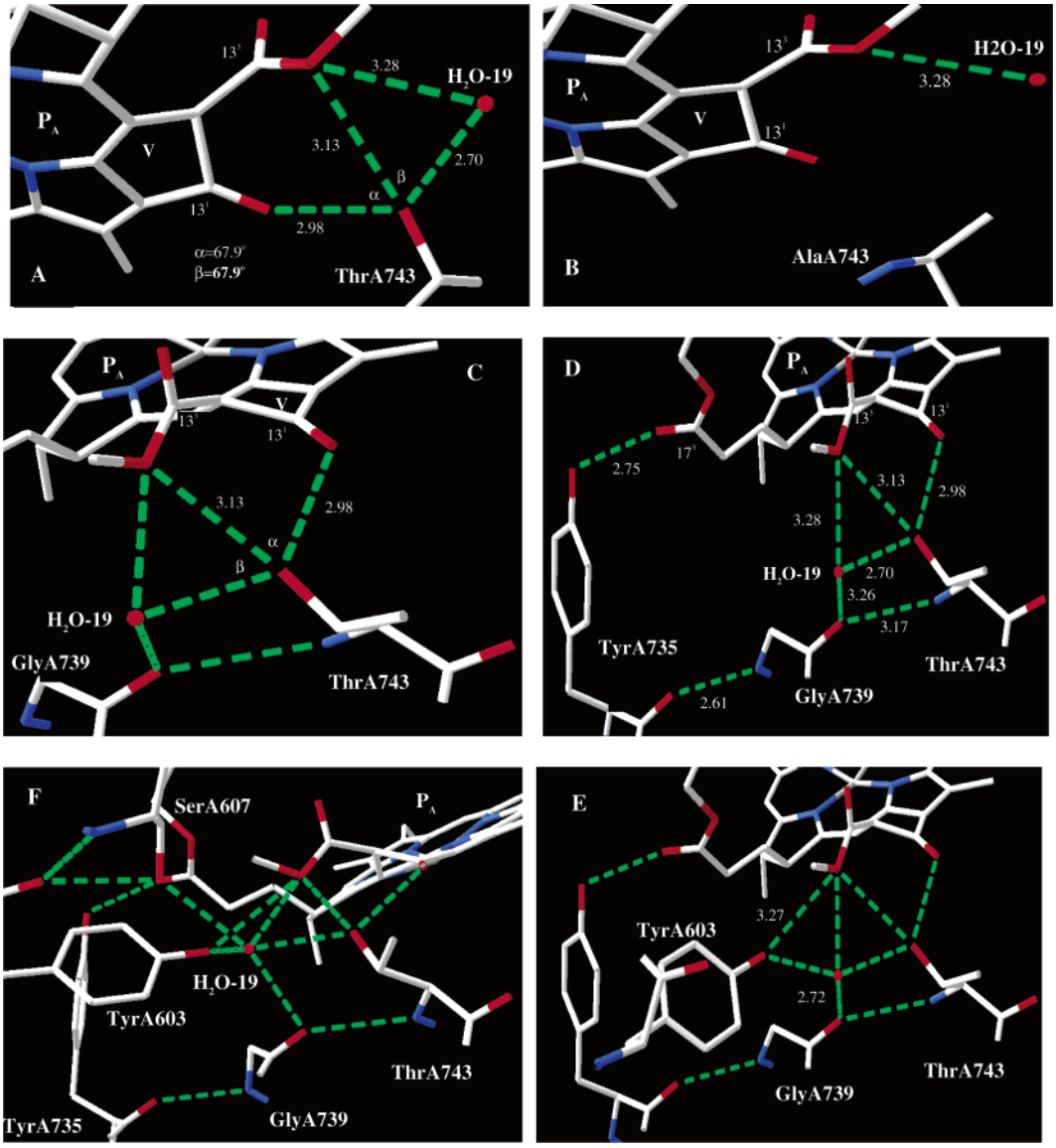

FIGURE 2: Several views of the molecular geometry around ring V of PA. Possible H-bonding interactions are shown (green, dotted). Figures were generated using Swiss PDBViewer and the crystallographic coordinates of PS I at 2.5 Å resolution (PDB IJB0). In panel A, ThrA743 (ThrA739 in *C. reinhardtii*) and a nearby water molecule (red circle) are shown. In panel B, the geometry when ThrA743 is changed to alanine is shown. (C) Another view of the same species as in panel A (except GlyA739), and possible hydrogen bonding interactions, are also shown. (D) Same species as in panel C with TyrA735, and possible hydrogen bonding interactions, are also shown. (E) Same species as in panel D with TyrA603, and possible hydrogen bonding interactions, are also shown. (F) Same species as in panel E with SerA607, and possible hydrogen bonding interactions, are also shown.

including the 2000−1770 cm^{-1} region. The 2000−1770 cm^{-1} region contains no difference bands. The lack of any features in the deconvolved spectra in the 2000−1770 cm^{-1} region is testimony to the appropriateness of the Fourier deconvolution procedures used (*15*−*17*).

RESULTS

Figure 3 shows ($P700^+$−P700) FTIR DS obtained using WT (top) and TA(A739) mutant (middle) PS I particles from *C. reinhardtii*, in the 1800−1200 cm^{-1} region. The [WT-TA(A739)] DDS is also shown (bottom). The spectra in Figure 3 were collected with the instrumental resolution set at 4 cm^{-1}. The mutant spectrum was scaled by a factor of 2.0. This scaling minimizes the amplitude of the bands in the DDS in the 7000−1200 cm^{-1} region (data not shown, but see Figure 3). Figures 4A and 5A show expanded views of the spectra in Figure 3, in the 1770−1700 and 1740−1580 cm^{-1} spectral regions, respectively. We have performed identical sets of measurements using PS I membranes, and the [WT-TA(A739)] DDS for both membranes and particles are identical (data not shown). This indicates that the PS I particle preparation procedures did not modify the molecular environment of P700 in the WT or the mutant.

The FTIR DDS in Figure 4A suggest that the positive difference band at 1753.7 cm^{-1} downshifts slightly upon mutation. Although the shift is observable in the FTIR DDS in Figure 4A, it is not well-resolved in the FTIR DS. To fully characterize the mutation induced band shifts in the 1770−1580 cm^{-1} spectral region, data was also collected at 2 cm^{-1} resolution, and these spectra are shown in Figures 4B and 5B.

The very high signal-to-noise ratio in our experiments allows effective application of Fourier deconvolution methods (*15*−*17*) to the spectra in Figure 5B. Figure 5C shows

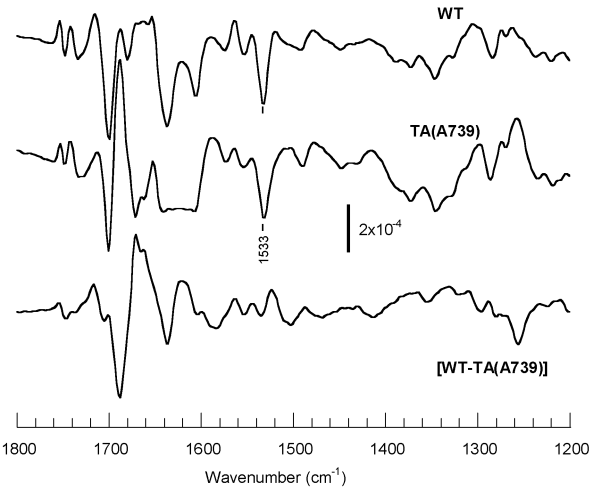

FIGURE 3: (A) (P700+−P700) FTIR DS obtained using WT (top) and TA739 (middle) PS I particles from *C. reinhardtii*, in the 1800−1200 cm^{-1} region. The [WT-TA(A739)] double difference spectrum is also shown (bottom). The mutant spectrum was scaled to the WT spectrum in a manner that minimizes the amplitude of the bands in the double difference spectrum in all spectral regions. Spectral resolution was 4 cm^{-1}.

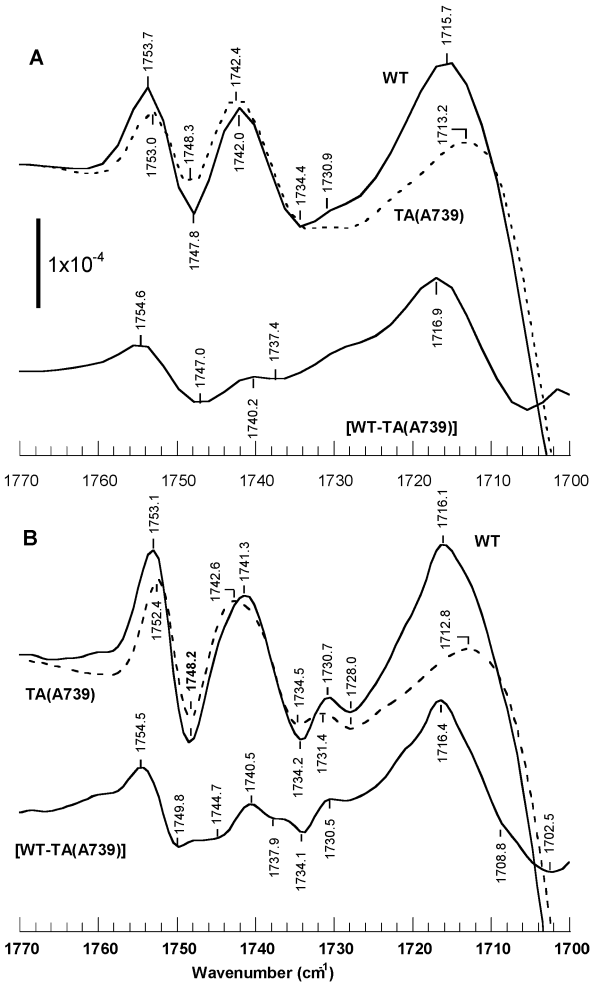

FIGURE 4: (A) (P700+−P700) FTIR DS obtained using WT (solid) and TA(A739) mutant (dotted) PS I particles from *C. reinhardtii*, in the 1770−1700 cm^{-1} region. These spectra were collected at 4 cm^{-1} resolution. The [WT-TA(A739)] DDS is also shown (bottom). (B) Same spectra as in panel A but collected at 2 cm^{-1} resolution.

the results of Fourier deconvolution of the FTIR DDS in Figure 5B. Similar results were obtained by first deconvolving the FTIR DS in Figure 5B and then obtaining the [WT-TA(A739)] FTIR DDS by subtraction (data not shown).

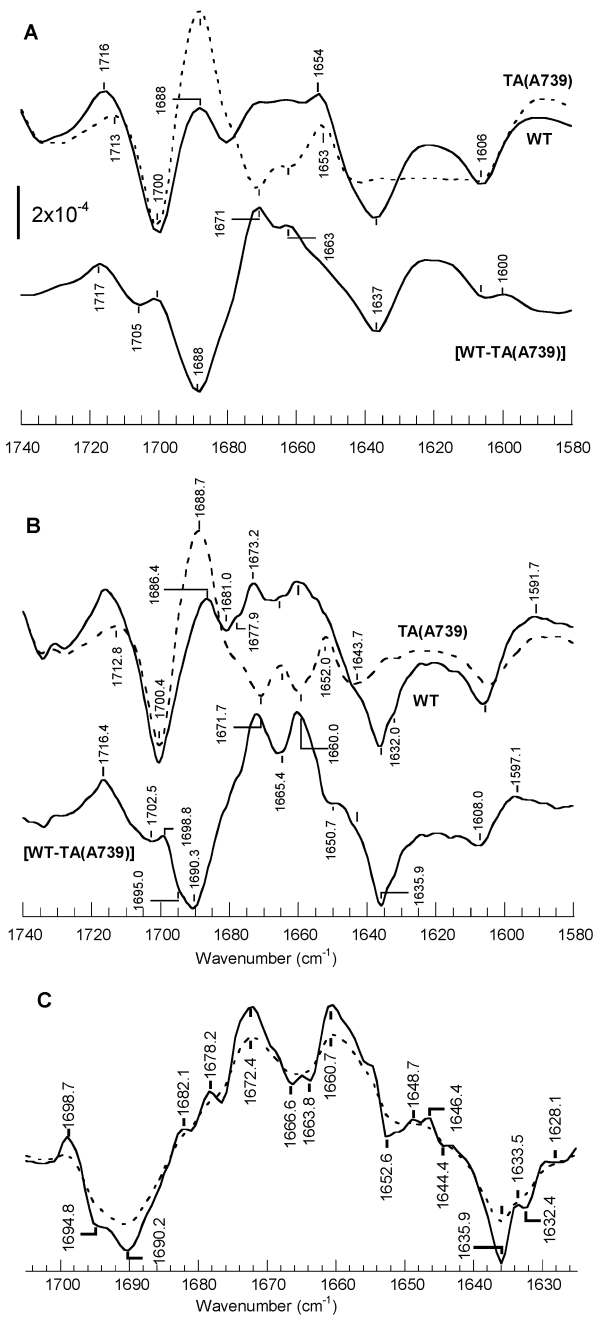

FIGURE 5: (A) (P700+−P700) FTIR DS obtained using WT (solid) and TA(A739) mutant (dotted) PS I particles from *C. reinhardtii*, in the 1740−1580 cm^{-1} region. The [WT-TA(A739)] DDS is also shown (bottom). Spectra were collected at 4 cm^{-1} resolution. (B) Same spectra as in panel A but collected at 2 cm^{-1} resolution. (C) Expanded view of the FTIR DDS shown in panel B (dotted). Also shown is the FTIR DDS obtained after Fourier deconvolution of the DDS in panel B (solid). Deconvolution parameters were bandwidth, 1.0 and resolution enhancement, 8 (deconvolution factor, 535; noise reduction factor, 4.5). See OPUS software notes from Bruker Instruments for details.

Deconvolution procedures are widely used to enhance the resolution of amide I and II absorption bands of proteins (*15*−*17*). This enhancement is a crucial step in estimating the component bands that underlie the amide I and II absorbance bands. Fourier deconvolution procedures have also been used to analyze protein secondary structural

changes in temperature induced FTIR DS (*18*, *19*). The Fourier deconvolution procedures applied here are limited by our instrumental resolution of 2 cm^{-1}. Thus, no bands in the deconvolved spectra can have a bandwidth less than 2 cm^{-1}. All of the bands in the FTIR DDS in Figure 5C are significantly greater than 2 cm^{-1}, and Fourier deconvolution has therefore been applied appropriately.

DISCUSSION

In ($P700^+$−P700) FTIR DS, negative bands correspond to modes of P700 (in the ground state) while positive bands correspond to modes of $P700^+$. One advantage of FTIR DS therefore is that it provides information on molecular modes of both P700 and $P700^+$ (*20*, *21*). In the ensuing discussion, we will distinguish between modes of P700 or $P700^+$. We will specify band peak frequencies to 0.1 cm^{-1}. These peak frequencies are found by interpolation. At 2 cm^{-1} resolution, however, the interval between data points is 0.62 cm^{-1}.

13^3 Ester C═Os. Much of the interpretation of bands in ($P700^+$−P700) FTIR DS is based on studies of modified Chls (*22*−*24*) and their corresponding cations (*25*) in organic solvents. Presently, it appears to be accepted that that the 1753.7(+)/1747.8(−) cm^{-1} difference band in WT FTIR DS (Figure 4A) is due to an upshift of the 13^3 ester C═O of P_B upon cation formation. For Chl-*a* in organic solvent, the 13^3 ester C═O absorbs at 1742 cm^{-1} and upshifts 12 cm^{-1} upon cation formation (*25*). In addition, the difference band at ∼1742.4(+)/1734.4(−) cm^{-1} (Figure 4A) is thought to be due to the 13^3 ester C═O of P_A. This difference band is not well-resolved at 4 cm^{-1} resolution. In the spectra collected at 2 cm^{-1} resolution, the difference band is clearly resolved, at 1741.3(+)/1734.2(−) cm^{-1}. In Figure 4B, a weak derivative feature is also clearly observed at 1730.7(+)/1728.0(−) cm^{-1} in the WT FTIR DS. The origin of this weak feature is not clear. It could be due to one or both of the 17^3 ester C═O modes of P_A and P_B. The ∼1731(+)/1728 cm^{-1} difference feature is weak because the 17^3 ester C═O is distantly located from the charge distribution over the Chl macrocycle.

The fact that there are two 13^3 ester C═O bands in ($P700^+$−P700) FTIR DS was taken as an indication that P700 is dimeric (*25*). The fact that they absorb at different frequencies indicates different environmental perturbations on each of these modes. It was suggested that the lowered frequency of the 13^3 ester C═O mode of P_A could indicate that it is H-bonded (*25*, *26*). However, the structural data in Figure 2 indicate that the 13^3 ester C═O of P_A is not H-bonded. Two mechanisms could account for the lowered frequency: (1) the 13^3 ester C═O is coupled to the bridging ester oxygen, which is H-bonded (Figure 2C). We note, however, that the ester oxygen is likely to be a weak H-bond acceptor (*11*). (2) The lowered frequency of the 13^3 ester C═O of P_A could also result from the fact that P_A is a Chl-*a*′ and/or the fact that ring V of P_A (unlike P_B) is considerably bent out of the plane of the macrocycle (Figure 2C,F).

Mutation Induced Alteration of the 13^3 and 17^3 Ester C═Os of P_A (P_A^+) and P_B (P_B^+). In the WT FTIR DS in Figure 4B, two difference bands are observed at ∼1753.1(+)/1748.2(−) and ∼1741.3(+)/1734.2(−) cm^{-1}. The negative bands at 1748.2(−) and 1734.2(−) cm^{-1} do not appear to shift upon mutation, although both bands appear slightly decreased in intensity. The positive band at 1753.1(+) is downshifted to 1752.4 cm^{-1} upon mutation, while the positive band at 1741.3(+) cm^{-1} upshifts to 1742.6 cm^{-1} (Figure 4B). Although the difference band shifts are small, they are clearly resolved, especially in the double difference spectrum in Figure 4B. The derivative feature at 1754.5(+)/1749.8(−) cm^{-1} in the DDS in Figure 4B is a very strong indication that only the positive band at 1753.1(+) cm^{-1} in the WT spectrum downshifts upon mutation, while the negative band at 1748.4 cm^{-1} does not shift. Similarly, the derivative feature at 1744.7(−)/1740.5(+) cm^{-1} in the DDS in Figure 4B indicates that the positive band at 1741.3(+) cm^{-1} in the WT FTIR DS upshifts upon mutation, while the negative band at 1734.2 cm^{-1} does not shift. The oppositely directed mutation induced shifts of the 1753.1(+) and 1741.3(+) cm^{-1} bands in the WT spectrum (Figure 4B) give rise to the decrease in intensity of the 1748.2 cm^{-1} difference band upon mutation. Given the assignments for the 13^3 ester C═O bands of P_A/P_A^+ and P_B/P_B^+ outlined previously (see also Table 1), these observations indicate that that the 13^3 ester C═O modes of P_B^+/P_A^+ downshift/upshift upon mutation, while the 13^3 ester C═O modes of P_B/P_A are unaffected by the mutation.

Table 1: Mutation Induced Shifts in Frequency of the C═O Modes of P700 and $P700^+$ Taken from Figures 4B and 5B

WT	TA(A739)	shift	assignment
1753.1	1752.4	−0.7	13^3 ester C═O of P_B^+
1748.2	1748.2	0	13^3 ester C═O of P_B
1741.3	1742.6	+1.3	13^3 ester C═O of P_A^+
1734.2	1734.2	0	13^3 ester C═O of P_A
1730.7	1734.1	+3.4	17^3 ester C═O of P_A^+
1728.0	1728.0	0	17^3 ester C═O of P_A
1716.1	1712.8	−3.3	13^1 keto C═O of P_B^+
∼1704.0	∼1704.0	0	13^1 keto C═O of P_B
1694.8	1698.7	+3.9	13^1 keto C═O of P_A
1686.4	1688.7	+2.3	13^1 keto C═O of P_A^+

Finally, the single derivative feature at 1734.1(−)/1730.5(+) cm^{-1} in the DDS in Figure 4B suggests that a positive difference band at 1730.7 cm^{-1} has upshifted to ∼1734.1 cm^{-1} in the mutant. The band at 1728.7(−) cm^{-1} appears to be little affected by the mutation. Above, we suggested that the 1730.7(+) cm^{-1} band in the WT FTIR DS in Figure 4B is due to one of the 17^3 ester C═Os. The fact that it upshifts upon mutation would then indicate that it is due to the 17^3 ester C═O of P_A^+.

The 1730.7(+) cm^{-1} band displays a mutation induced upshift that is larger than the shifts observed for the 13^3 ester C═O difference bands. This most likely indicates some modulation of the H-bond network in the vicinity of the 17^3 ester C═O of P_A, as it is unlikely that a charge redistribution within P_A^+ and P_B^+ would significantly impact the mode frequency of the 17^3 ester C═O of P_A. If the H-bond network is modified, then this suggests that ThrA739 is coupled to the network. This then indicates that it is likely that the water molecule H-bonds to the side chain hydroxyl oxygen of ThrA739.

From electrochemical studies of Chl-*a* and Chl-a^+, it is known that the 13^3 ester C═O modes increase in frequency upon cation formation. For example, the ester difference bands in Figure 4A upshift upon cation formation. These observations suggest that absorption frequencies of the ester

C═O groups of Chls will decrease/increase as the amount of positive charge on the Chl decreases/increases. Therefore, the mutation induced shifts of the difference bands in Figure 4 suggest (1) the electronic configuration of P700 in the vicinity of the 13^3 and 17^3 ester C═Os is unaltered by the mutation. (2) In the mutant, the positive charge over P_A^+ and P_B^+ is distributed differently from that of WT. Charge on P_B^+ in the mutant is reduced relative to that of WT, while charge on P_A^+ in the mutant is increased relative to WT. That is, mutation of ThrA739 to alanine modifies $P700^+$, with charge on P_B being relocated onto P_A. This model is in good agreement with mutation induced changes associated with the 13^1 keto C═O mode of P_B^+ (see below).

In passing, we note that the oppositely directed mutation induced shifts of the 1753.1(+) and 1741.3 difference bands provide direct evidence that these bands are due to different 13^3 ester C═O modes. Thus, we provide the first direct evidence that the two difference bands above ~1730 cm^{-1} in the WT FTIR DS are due to 13^3 ester C═O modes of different pigments and that these bands are not due to some type of mode frequency heterogeneity, as has been suggested (*28*). Finally, we stress that there are very few mechanisms that could explain the mutation induced frequency decrease of the 13^3 ester C═O of P_B^+. Generally, when a species interacting with a C═O group is removed, the C═O absorption frequency will increase. So the downshift of the 13^3 ester C═O of P_B^+ is very strong evidence supporting the above-described mutation induced charge redistribution within the pigments of $P700^+$. This charge redistribution can explain the upshift of the 13^3 ester C═O of P_A^+. However, this upshift could also be (perhaps partially) due to modulation of the H-bond network near the 13^3 ester oxygen of P_A.

Mutation Induced Alteration of the 13^1 Keto C═O of P_B (P_B^+). The data in Figure 4 indicate that mutation of ThrA739 to Ala results in a charge redistribution over the pigments in the $P700^+$ state. Given this, we would predict that the mutation will decrease the frequency of the 13^1 keto C═O mode of P_B^+.

One interpretation of WT ($P700^+$−P700) FTIR DS is that the 1700(−) cm^{-1} band of WT (Figure 5A) is due to the 13^1 keto C═O of P_B, which upshifts to ~1716 cm^{-1} upon cation formation (*29*). Within this interpretation, the 1637(−) cm^{-1} band is proposed to be due to the 13^1 keto C═O of P_A, which upshifts to ~1654 cm^{-1} upon cation formation. The origin of the 1688(+) cm^{-1} band is not considered in this model. In an alternative interpretation of WT ($P700^+$−P700) FTIR DS, we proposed that the 1700(−) cm^{-1} band is due to the 13^1 keto C═Os of both P_B and P_A, at ~1703 and ~1697 cm^{-1}, respectively (*14*). The ~1703 cm^{-1} band of P_B upshifts to ~1716 cm^{-1} upon cation formation, while the ~1697 cm^{-1} band of P_A downshifts to ~1687 cm^{-1} (*14*). We also suggested that the 1636(−)/1654(+) cm^{-1} difference band is due to modes associated with the axial histidine ligands (HisA676 and B656 in *C. reinhardtii*).

The band-shifts discussed previously are better resolved at 2 cm^{-1} resolution: in Figure 4B, the 1716.1(+) cm^{-1} band of WT clearly downshifts to 1712.8 cm^{-1} and decreases considerably in intensity upon mutation. This downshift results in a single derivative feature at 1716.4(+)/1702.5 cm^{-1} in the FTIR DDS in Figure 5B. The fact that only a single derivative feature is observed indicates that it is only the positive band at 1716.1(+) cm^{-1} that is affected by the mutation and is downshifted ~3.3 cm^{-1}.

From hybrid density functional calculations of the vibrational structure of Chl-*a* and Chl-a^+, it has been demonstrated that the 13^1 keto C═O mode frequency is related in an approximately linear fashion to the amount of charge on the Chl. The more positive the charge on the Chl, the higher the frequency (*30*). These calculations therefore predict that absorption frequencies of non-H-bonded 13^1 keto C═O groups of Chls will decrease/increase as the amount of positive charge on the Chl decreases/increases. Therefore, the mutation induced downshift of the 1716.4(+) cm^{-1} difference band (Figure 5B) provides very strong evidence to support the hypothesis that the positive charge over P_B^+ in the mutant is decreased, relative to WT.

Witt et al. (*11*) have used ENDOR spectroscopy to study WT PS I from *C. reinhardtii* (strain CC2696) and mutants in which ThrA739 was changed to tyrosine, histidine, or valine. The hyperfine coupling constant for the methyl group at position 12 of P_B was impacted the most by the mutations. From this observation, Witt et al. suggested a spin redistribution within $P700^+$. It is not clear if this spin redistribution was localized to P_B or extended over P_A also. The above-described mutation induced charge redistribution between P_A^+ and P_B^+ suggests that the mutation induced changes in the hyperfine coupling constants observed by Witt et al. probably arise because of a spin redistribution between P_B and P_A.

From a variety of curve fitting simulations (data not shown), we have found that a single mutation induced shift of the positive 1716.1 cm^{-1} band in the WT FTIR DS (Figure 5B) cannot simultaneously explain the mutation induced decrease in intensity of the 1716.1 cm^{-1} band (Figure 5B) and the negative feature at 1702.5 cm^{-1} in the FTIR DDS in Figure 5B. Both features can be simulated adequately, however, if a negative band is included at ~1704 cm^{-1} that is unaffected by the mutation. We therefore conclude that a negative band is present near 1704 cm^{-1} in both FTIR DS in Figure 5B. We assign this band to the 13^1 keto C═O of P_B (Table 1). With these assignments, the FTIR DDS in Figure 5 are consistent with the band assignments that we previously proposed for P_B and P_B^+ (*14*).

Mutation Induced Alteration of the 13^1 Keto C═O of P_A. The 1700.4(−) cm^{-1} difference band of WT appears somewhat altered in the mutant spectrum (Figure 5B), but a negative band is still observed at 1700.4 cm^{-1}. This band is sharper in the mutant spectrum, however. This mutation induced band sharpening can be rationalized by an upshift of a negative band near 1696 cm^{-1} upon mutation. In the FTIR DDS spectrum in Figure 5B, a shoulder is observed at ~1695 cm^{-1}, while a positive band is observed at ~1698.8 cm^{-1}. In the resolution enhanced FTIR DS in Figure 5C, these features are clearly resolved, and a derivative feature is found at 1694.8(−)/1698.7(+) cm^{-1}. This derivative feature indicates that a negative band at ~1695 cm^{-1} has upshifted upon mutation. Previously, we suggested that a band at ~1697 cm^{-1} is due to the 13^1 keto C═O of P_A, so the above observation suggests that the negative band at 1694.8(−) cm^{-1} in the deconvolved FTIR DDS in Figure 5C is due to the 13^1 keto C═O of P_A, which upshifts 3.9 cm^{-1} upon mutation (Table 1). The upshift of the 1694.6-(−) cm^{-1} band is an indication that the 13^1 keto C═O of P_A

(in the ground state) is slightly modified in the mutant. Since the 13^1 keto C═O of P_B is unaltered by the mutation, the mutation induced modification of the 13^1 keto C═O of P_A most likely results because of a change in the H-bond network.

In the WT FTIR DS, we suggest that a negative band at ~1695 cm^{-1} downshifts to ~1688 cm^{-1} upon cation formation. This downshift results from a strengthening of the H-bond to the 13^1 keto C═O of P_A. Below, we will show that cation formation also induces a downshift of the band associated with the 13^1 keto C═O of P_A in the mutant. This means that an H-bond to the 13^1 keto C═O of P_A is also present in the mutant. Consistent with this idea is the observation that the mutation induced shift in the band associated with the 13^1 keto C═O of P_A is small.

Finally, it is very difficult to describe the FTIR DDS in the 1720−1690 cm^{-1} region without the 1700(−) cm^{-1} band in WT FTIR DS containing contributions from at least two negative component bands. This is consistent with our previous findings (*14*).

Mutation Induced Alteration of the 13^1 Keto C═O of P_A^+. In the FTIR DS in Figure 5B, it appears that a positive band at 1686.4(+) cm^{-1} in the WT spectrum has upshifted 2.3 cm^{-1} to 1688.7 cm^{-1} upon mutation. The 1686.4(+) cm^{-1} band in the WT spectrum has also increased considerably in intensity. This intensity increase can be partly explained by the upshift of the negative 1694.8 cm^{-1} band, discussed previously. The mutation induced upshift of the positive 1686.4 cm^{-1} band in the WT spectrum to 1688.7 cm^{-1} in the mutant can also explain, at least in part, the negative band at 1690.4 cm^{-1} in the FTIR DDS in Figure 5C and the positive bands at 1682.3 or 1678.0 cm^{-1}. Irrespective of which of the two bands, we associate the 1686.4(+) cm^{-1} feature in the WT FTIR DS (Figure 5B) with the 13^1 keto C═O of P_A^+. This again is compatible with our previous interpretation of FTIR DS (*14*).

Previously, we suggested that the 13^1 keto C═O mode of P_A downshifted, to ~1686 cm^{-1}, upon cation formation. This downshift was rationalized via the notion that the H-bond to the 13^1 keto C═O mode of P_A became stronger in the $P700^+$ state (*14*). Given that the mutation induced upshift of the 1686.4(+) cm^{-1} band is only ~2−3 cm^{-1}, the suggestion is that an H-bond must also be present in the TA(A739) mutant.

In summary, the spectra in Figure 5 are compatible with our previous assignments of FTIR difference bands associated with the 13^1 keto C═O modes of P_A (P_A^+) and P_B (P_B^+). However, this is likely to be the case only if an H-bond to the 13^1 keto C═O of P_A is still present in the TA(A739) mutant. Witt et al. have also concluded that an H-bond is still present in all three of their TA739 mutants (*11*). The H-bond in the mutant is possibly mediated by an introduced water molecule. If a water molecule is introduced into the P700 binding site in the mutant, then this could give rise to derivative feature in the FTIR DDS, in the ~1660−1620 cm^{-1} region, because of new H−O−H bending modes (*31*) in the mutant.

Mutation Induced Alteration of Protein Modes. To fully explain the positive intensity of the 1688.7(+) cm^{-1} band in the mutant FTIR DS (Figure 5B), it is likely that further modes must be altered upon mutation. The FTIR DS and DDS in Figure 5C do indicate that bands in the ~1682−1678 cm^{-1} region are altered upon mutation.

Although not resolved in Figure 5A, a difference band is clearly observed at 1673.2(+) cm^{-1} in the WT FTIR DS (Figure 5B). This band appears to downshift to ~1665.4(+) cm^{-1} (or possibly 1652.0 cm^{-1}) upon mutation. This shift results in the positive feature at 1671.7 cm^{-1} in the FTIR DDS in Figure 5B. This downshifting difference band could be associated with a protein mode that is altered upon mutation. Given the protein environment around P_A (Figure 2), this idea is reasonable.

Can the 1637(−)/1654(+) cm^{-1} Difference Band in the WT FTIR DS in Figure 5A Be Due to the 13^1 Keto C═O of P_A? Previously, it has been suggested that the 1637(−)/1654(+) cm^{-1} difference band in WT FTIR DS (Figure 5A) is due to the 13^1 keto C═O of P_A, at least in *S. 6803* (*29*). Such a low frequency for the 13^1 keto C═O was suggested to result from the presence of an extremely strong H-bond to the C═O. If this interpretation is correct, then the whole of the 1637(−)/1654(+) cm^{-1} difference band should downshift considerably upon uniform ^2H labeling of PS I. No such complete difference band downshift is observed (*29*) (G. Hastings, manuscript submitted), and this interpretation is therefore unlikely.

If the 1637(−)/1654(+) cm^{-1} difference band were due to a strongly H-bonded 13^1 keto C═O of P_A, then removal of this strong H-bond would cause the 1637(−)/1654(+) cm^{-1} difference band to upshift considerably, possibly by as much as 60 cm^{-1}. The FTIR DDS in Figure 5A shows a set of features at 1637(−)/1663(+)/1671(+)/1688(−) cm^{-1}. These features in the DDS in Figure 5A could suggest the following: a difference band at 1637(−)/1663 cm^{-1} is present in the WT spectrum and shifts ~34/26 cm^{-1} to ~1671(−)/1688(+) cm^{-1} upon mutation. That is, the 1637(−) cm^{-1} band in the WT FTIR DS upshifts 26 cm^{-1} upon cation formation. In contrast, the 1671(−) cm^{-1} band in the mutant spectrum upshifts 17 cm^{-1}, to ~1688 cm^{-1}, upon cation formation. These observations could suggest the removal of a strong H-bond from the 13^1 keto C═O of P_A. However, several observations suggest otherwise: (1) the 1671 cm^{-1} band (proposed to be due to the 13^1 keto C═O of P_A in the mutant) upshifts 17 cm^{-1} upon cation formation. Therefore, the upshift upon cation formation in the mutant is significantly less (by 9 cm^{-1}) than in WT. This suggests that the charge on P_A^+ in the mutant is much less than in WT. However, above we showed that the mutation resulted in charge being redistributed within $P700^+$, with charge from P_B^+ being relocated onto P_A^+. Given this, we would then expect that the cation induced upshift in the mutant would be greater than 26 cm^{-1}, as compared to an observed shift of only ~17 cm^{-1}. The interpretation outlined above (that the quadruple feature at 1637(−)/1663(+)/1671(+)/1688(−) cm^{-1} in the DDS in Figure 5A is due to the loss of an H-bond to the 13^1 keto C═O mode of P_A) is therefore incompatible with the changes in the 13^3 ester C═O region, as well as the changes associated with the 13^1 keto C═O of P_B^+. The same conclusions can also be drawn by considering the spectra collected at higher resolution (Figure 5B): a difference band at 1635.9(−)/1660.0(+) cm^{-1} in the WT FTIR DS upshifts to 1671.7(−)/1690.3 cm^{-1} in the mutant. That is, in WT, a cation induced upshift of 24.1 cm^{-1} is observed. In the mutant, a cation induced upshift of 18.6

cm^{-1} is observed. Again, the cation induced upshift is significantly less in the mutant than in WT. As pointed out above, this is not compatible with a greater positive charge on P_A^+ in the mutant as compared to WT. (2) In the ThrA739 mutant, the 13^1 keto C═O of P_A is now presumably free from H-bonding. However, an absorption frequency of ~1671 cm^{-1} for a free 13^1 keto C═O mode is rather low. (3) It is likely that the positive band at 1673.2 cm^{-1} in the WT FTIR DS (Figure 5B), which is not resolved at lower resolution (Figure 5A), gives rise to the 1671.7(+) cm^{-1} feature in the FTIR DDS (Figure 5B). The above three observations therefore lead us to the conclusion that the mutation induced changes in the 1630−1690 cm^{-1} region are not related to a large upshift of a difference band associated with the 13^1 keto C═O mode of P_A.

Mutation Induced Alteration of the Axial Histidine Ligands. Previously, we suggested that the ~1637(−)/1654 cm^{-1} difference band in WT FTIR DS (Figure 5A) is due to both HisA676 and HisB656. More specifically, the difference band is due to the C_4═C_5 modes of the histidine imidazoles that are protonated at one nitrogen and involved in metal binding at the other (*14*). The shoulder observed at 1632.0 cm^{-1} in the WT FTIR DS in Figure 5B supports the idea that at least two negative components contribute to the ~1637(−) cm^{-1} difference band.

The negative band at 1608 cm^{-1} in the WT FTIR DS (Figure 5B) is clearly downshifted upon mutation (Figure 5B). It is thought that this band is indicative of pentacoordinated Chl-*a* (*32*, *33*). The fact that the 1608 cm^{-1} band is modified upon mutation therefore suggests some coordination modifications of P_A and P_B. If the coordinating histidine ligands to P700 are modified, and the band at ~1637(−) cm^{-1} is due to both ligating histidines, then the ~1637(−) cm^{-1} band would be expected to be modified upon mutation. The histidine ligands of P700 could be modified because the mutation disrupts the conformation of the macrocycles of P_A and/or P_B or because the charge distribution over the Chls is changed in the mutant.

The FTIR DDS at 2 cm^{-1} resolution in Figure 5B shows several shoulders that indicate underlying unresolved structure in the spectra. To investigate this underlying structure, we have used Fourier deconvolution methods to enhance the resolution of the FTIR DDS in Figure 5B. The resolution enhanced FTIR DDS is shown in Figure 5C.

Clearly, the mutation considerably impacts the 1635.9(−) cm^{-1} difference band. The 1635.9(−) cm^{-1} difference band is almost completely lost in the mutant spectrum. It could be possible that a difference band at ~1636(+)/1629(−) cm^{-1} is present in the mutant spectrum because of an H−O−H bending mode of an introduced water molecule, for example. If this is the case, then it would be difficult to observe changes in ground-state modes of the axial histidines in the FTIR DDS.

Notwithstanding the above, the resolution enhanced FTIR DDS in Figure 5C suggest that a negative difference band at 1632.4 cm^{-1} downshifts upon mutation, while the 1635.9(−) cm^{-1} difference band upshifts to near 1644 cm^{-1}. Since the 1635.9(−) cm^{-1} difference band in the WT FTIR DS upshifts upon mutation, it is likely that it is associated with HisA676. Similarly, since the band near 1632(−) cm^{-1} downshifts upon mutation, we associate it with HisB656.

If the 1635.9(−)/1660.0(+) cm^{-1} difference band in WT FTIR DS is due to both axial histidines, then the 1660.0(+) cm^{-1} band should split in the mutant FTIR DS because charge is redistributed between P_A and P_B in the mutant. The features at 1663.8(−)/1660.7(+)/1652.6(−) cm^{-1} in the resolution enhanced FTIR DDS (Figure 5C) indicate that this hypothesis could be appropriate. That is, the 1663.8(−)/1660.7(+) cm^{-1} derivative feature in the deconvolved FTIR DDS (Figure 5C) is due to a mutation induced upshift of a positive band near 1660.0(+) cm^{-1}. The 1663.8 cm^{-1} feature in the deconvolved FTIR DDS (Figure 5C) is then due to HisA676. The 1660.7(+)/1652.6(−) cm^{-1} derivative feature in the deconvolved FTIR DDS is due to a mutation induced downshift of part of the 1660.0(+) cm^{-1} band in the WT FTIR DS. Similarly, the 1652.6 cm^{-1} feature in the deconvolved FTIR DDS is then due to HisB656.

Conclusions. The 13^3 ester and 13^1 keto C═O modes of P_B^+ downshift when ThrA739 is changed to alanine. In contrast, the 13^3 ester C═O mode of P_A^+ upshifts upon mutation. These shifts indicate that the mutation alters the delocalized charge distribution in the $P700^+$ state, with charge on P_B being relocated onto P_A in the mutant. The rationale behind substituting ThrA739 with Ala was to remove the proposed H-bond to the 13^1 keto C═O of P_A. However, an H-bond still appears to be present in the mutant, probably mediated via an extra water molecule that is introduced into mutant PS I but is not present in WT PS I. The mutation induced changes in the ($P700^+$−P700) FTIR DS are compatible with FTIR difference band assignments that we proposed recently (*14*).

REFERENCES

1. Walker, D. (1993) *Energy, plants and man*, 2nd ed., Oxygraphics, Mill Valley, CA.
2. Blankenship, R. E. (2002) *Molecular mechanisms of photosynthesis*, Blackwell Science, Malden, MA.
3. Ke, B. (2001) *Photosynthesis: photobiochemistry and photobiophysics*, Vol. 10, Kluwer Academic Publishers, Dordrecht, The Netherlands.
4. Golbeck, J. H., and Bryant, D. (1991) *Current topics in bioenergetics*, pp 83−175, Academic Press, New York.
5. Purton, S., Stevens, D. R., Muhiuddin, I. P., Evans, M. C., Carter, S., Rigby, S. E., and Heathcote, P. (2001) *Biochemistry 40*, 2167−2175.
6. Muhiuddin, I. P., Heathcote, P., Carter, S., Purton, S., Rigby, S. E., and Evans, M. C. (2001) *FEBS Lett. 503*, 56−60.
7. Boudreaux, B., MacMillan, F., Teutloff, C., Agalarov, R., Gu, F., Grimaldi, S., Bittl, R., Brettel, K., and Redding, K. (2001) *J. Biol. Chem. 276*, 37299−37306.
8. Joliot, P., and Joliot, A. (1999) *Biochemistry 38*, 11130−11136.
9. Jordan, P., Fromme, P., Witt, H. T., Klukas, O., Saenger, W., and Krauss, N. (2001) *Nature 411*, 909−917.
10. Fromme, P., Jordan, P., and Krauss, N. (2001) *Biochim. Biophys. Acta−Bioenerg. 1507*, 5−31.
11. Witt, H., Scholdder, E., Teutloff, C., Niklas, J., Bordignon, E., Carbonera, D., Kohler, S., Labahn, A., and Lubitz, W. (2002) *Biochemistry 41*, 8557−8569.
12. Redding, K., MacMillan, F., Leibl, W., Brettel, K., Rutherford, A. W., Breton, J., and Rochaix, J.-D. (1988) in *Photosynthesis: Mechanisms and Effects* (Garab, G., Ed.) pp 591−594, Kluwer Academic Publishers, Dordrecht, The Netherlands.
13. Harris, E. H. (1989) *The Chlamydomonas sourcebook: a comprehensive guide to biology and laboratory use*, Academic Press, San Diego.
14. Hastings, G., Ramesh, V. M., Wang, R., Sivakumar, V., and Webber, A. (2001) *Biochemistry 40*, 12943−12949.
15. Surewicz, W., and Mantsch, H. (1996) in *Spectroscopic methods for determining protein structure in solution* (Havel, H., Ed.) pp 135−162, VCH, New York.

16. Yang, J. J., Yang, H., Ye, Y., Hopkins, H., Jr., and Hastings, G. (2002) *Cell Biochem. Biophys. 36*, 1−18.
17. Jackson, M., and Mantsch, H. H. (1995) *Crit. Rev. Biochem. Mol. Biol. 30*, 95−120.
18. Fabian, H., Schultz, C., Backmann, J., Hahn, U., Saenger, W., Mantsch, H. H., and Naumann, D. (1994) *Biochemistry 33*, 10725−10730.
19. Fabian, H., and Mantsch, H. H. (1995) *Biochemistry 34*, 13651−13655.
20. Nabedryk, E. (1996) in *Infrared spectroscopy of biomolecules* (Mantsch, H. H., and Chapman, D., Eds.) pp 39−81, Wiley-Liss, New York.
21. Mäntele, W. (1995) in *Anoxygenic Photosynthetic Bacteria* (Blankenship, R. E., Madigan, M. T., and Bauer, C. E., Eds.) pp 627−647, Kluwer Academic Publishers, Dordrecht, The Netherlands.
22. Katz, J. J., Dougherty, R. C., and Boucher, L. (1966) in *The chlorophylls* (Vernon, L. P., and Seely, G. R., Eds.) pp 185−251, Academic Press, New York.
23. Ballschmiter, K., Cotton, T. M., Strain, H. H., and Katz, J. J. (1969) *Biochim. Biophys. Acta 180*, 347−359.
24. Katz, J. J., Shipman, L., Cotton, T., and Janson, T. R. (1978) in *The Porphyrins. Physical Chemistry, Part C* (Dolphin, D., Ed.) pp 402−458, Academic Press, New York.
25. Nabedryk, E., Leonhard, M., Mantele, W., and Breton, J. (1990) *Biochemistry 29*, 3242−3247.
26. Breton, J. (2001) *Biochim. Biophys. Acta 1507*, 180−193.
27. Webber, A. N., and Lubitz, W. (2001) *Biochim. Biophys. Acta 1507*, 61−79.
28. Kim, S., and Barry, B. A. (2000) *J. Am. Chem. Soc. 122*, 4980−4981.
29. Breton, J., Nabedryk, E., and Leibl, W. (1999) *Biochemistry 38*, 11585−11592.
30. O'Malley, P. (2000) *J. Am. Chem. Soc. 122*, 7798−7801.
31. Smith, B. C. (1999) *Infrared spectral interpretation: a systematic approach*, CRC Press, Boca Raton, FL.
32. Fujiwara, M., and Tasumi, M. (1986) *J. Phys. Chem. 90*, 250−255.
33. Breton, J., Xu, W., Diner, B. A., and Chitnis, P. R. (2002) *Biochemistry 41*, 11200−11210.

BI034230C